Characterisation of electromagnetically coupled superquadric loop antennas for mobile communications applications

M.A. Jensen
Y. Rahmat-Samii

Indexing terms: Antenna diversity, Loop antennas, Superquadrics

Abstract: Analysis of two mutually coupled loop antennas with arbitrary relative orientation and position and possibly different geometries is presented. The antennas are represented by generalised superquadric curves, which include circular, elliptical, and rectangular loop geometries, and they may be located either in a homogeneous region or next to an infinite ground plane. A Galerkin-type moment method with piecewise sinusoidal subsectional basis and weighting functions is used. Special consideration is given to implement the solution using curved wire segments instead of the commonly employed linear segments to improve computational efficiency. This very general computational tool is used to investigate the behaviour of coupled loops in configurations suitable for personal communications applications. A discussion of the use of antenna diversity to increase the received signal-to-noise ratio for communications equipment used in a multipath fading environment is also presented. Computational examples show that antenna diversity can provide significant improvements even for closely spaced loop antennas used in mobile communications applications.

1 Introduction

The increasing effort in miniaturisation of mobile communications equipment has spurred the development of small, low-profile antennas suitable for implementation in portable devices. In many instances, the circular or noncircular loop antenna provides an efficient radiator for the application. Whereas in the past a single antenna element has been used for mobile transceivers, the desire to combat multipath fading has led to the use of multiple elements arranged in a suitable diversity scheme. When more than one element is used, an important design consideration is the effect of mutual coupling on the antenna performance. The work presented here has been performed to provide an understanding of the behaviour of electrically coupled circular and noncircular loop radiators with arbitrary relative positions and orientations.

Paper 9904H (E11), first received 19th February and in revised form 10th August 1993

The authors are with the Department of Electrical Engineering, University of California, Los Angeles, 405 Hilgard Avenue, Los Angeles, CA, 90024-1594, USA

To our best knowledge, there has not been a unified solution methodology allowing analysis of very generally shaped loops with arbitrary orientations and positions. Past research efforts have to some extent addressed issues related to this work and have provided useful design data. For example, several theoretical investigations into the behaviour of circular loop antennas have been performed using a Fourier series expansion for the loop current distribution [1–7]. This analysis has been extended to the case of two identical, parallel loops arranged in either a coaxial arrangement [8] or with offset axes [9] to determine the mutual impedance between the elements. The characteristics of polygonal loops comprised of linear wire segments have been evaluated using a moment method solution approach [10]. The effects of relative antenna position and orientation on the mutual coupling between two closely spaced dipole antennas has also been demonstrated [11].

In this work, we present a unified formulation which can be used to characterise not only circular loops but also numerous other geometrical configurations, including square loops and folded dipoles, through use of the mathematical construction of the superquadric curve [12]. The methodology allows analysis of two coupled superquadric loops of possibly different geometries and with completely arbitrary relative orientation and position, located either in a homogeneous medium or near an infinite ground plane. The solution technique employs a piecewise sinusoidal Galerkin moment method [13] to determine the antenna current distribution from a coupled electric-field integral equation (EFIE) for thin wires [14]. By performing the integrations necessary for the moment method implementation along the curved path representing the antenna, the accuracy and efficiency of the formulation is enhanced [15]. The current obtained is subsequently used to find the self and mutual impedances, input impedance, directivity, and radiation pattern for the coupled-loop antennas. Both magnetic frill and delta gap source models are employed to allow investigation of different possible feeding scenarios.

Following presentation of the preliminary mathematical derivations associated with the superquadric curve geometry and moment-method solution, attention is turned to the concept of antenna diversity to mitigate the effects of multipath fading at a mobile terminal [16–19].

This work is funded by ARPA contract DAAB07-93-C-C501. M. Jensen's work is also supported under a National Science Foundation graduate fellowship.

Several key expressions are presented which provide a quantitative measure of the diversity performance of coupled antennas. Computational results for several representative isolated and coupled-loop configurations are then provided to illustrate the accuracy and flexibility of the solution methodology and to provide an understanding of the behaviour of loop antennas designed for wireless personal communications system applications.

2 Superquadric representation for loops

A superquadric curve [12] is the locus of points satisfying the equation

$$\left|\frac{x}{a}\right|^v + \left|\frac{y}{b}\right|^v = 1 \tag{1}$$

where a and b are the semiaxes in the x and y-directions, respectively, and v is a squareness parameter which controls the behaviour of the loop radius of curvature. A parametric representation for the superquadric curve is provided in Section 8. Fig. 1 illustrates the effect of the squareness parameter by presenting the curve geometry

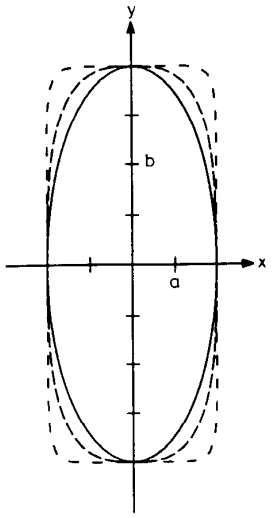

Fig. 1 *Superquadric geometry with aspect ratio of $b/a = 2$*
——— $v = 2$
– – – – $v = 3$
------- $v = 10$

for $v = 2$, 3, and 10 and an aspect ratio of $b/a = 2$. As can be seen from this Figure, a value of $v = 2$ corresponds to an ellipse while the loop squareness increases with v. It is evident that the superquadric representation allows modelling of numerous different loop configurations through variation of the shape parameters a, b, and v. Also, the model's capability to provide rounded corners on otherwise rectangular loops allows accurate representation of many practical geometries. This flexibility in geometrical configuration selection can be very useful for antenna packaging considerations.

Fig. 2 presents the geometry for the two coupled superquadric loops. Each loop is positioned in its own co-ordinate frame with the subscripts 1 and 2 denoting parameters associated with loops 1 and 2, respectively. The translation vectors r_{01} and r_{02} and the Eulerian angles [20] $(\alpha_1, \beta_1, \gamma_1)$ and $(\alpha_2, \beta_2, \gamma_2)$ designate the positions and orientations, respectively, of each loop co-ordinate frame with respect to the reference co-ordinate system. The co-ordinates s_1 and s_2 are the lengths of the curves measured from the feed points situated on each positive x-axis. The proper transformations required to

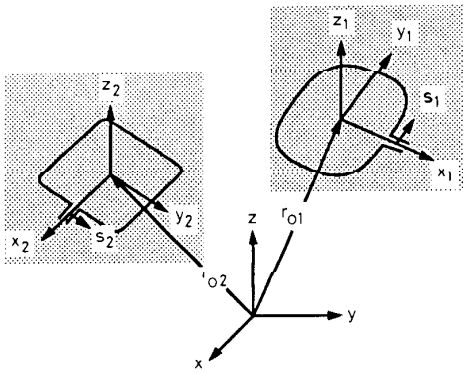

Fig. 2 *Geometry of two coupled loop antennas showing co-ordinates*

relate the loop co-ordinate systems to the reference frame in terms of the Eulerian angles and translation vectors are provided in Reference 20.

3 Moment method solution

3.1 Integral equation formulation

Analysis of the coupled superquadric loop antennas begins with the development of integral equations relating the currents on the wires to the excitation field applied at the antenna feed points. To formulate these integral equations, we used a thin-wire assumption which approximates the surface current density on the loops as filamentary currents $I_1(s_1)$ and $I_2(s_2)$ which flow in the axial directions only. The thin-wire form of the electric-field integral equation [14] can be manipulated to incorporate the effects of mutual coupling between the two loops as in

$$\begin{aligned}
&\hat{s}_1 E^{inc}(s_1) \\
&\quad = \frac{-1}{4\pi j\omega\varepsilon_0}\left\{\int_{L_1}\left[k_0^2\hat{s}_1\hat{s}_1' I_1(s_1')G_{11} + \frac{\partial I_1(s_1')}{\partial s_1'}\frac{\partial G_{11}}{\partial s_1}\right]ds_1'\right. \\
&\qquad \left. + \int_{L_2}\left[k_0^2\hat{s}_1\hat{s}_2' I_2(s_2')G_{12} + \frac{\partial I_2(s_2')}{\partial s_2'}\frac{\partial G_{12}}{\partial s_1}\right]ds_2'\right\} \\
&\hat{s}_2 E^{inc}(s_2) \\
&\quad = \frac{-1}{4\pi j\omega\varepsilon_0}\left\{\int_{L_1}\left[k_0^2\hat{s}_2\hat{s}_1' I_1(s_1')G_{21} + \frac{\partial I_1(s_1')}{\partial s_1'}\frac{\partial G_{21}}{\partial s_2}\right]ds_1'\right. \\
&\qquad \left. + \int_{L_2}\left[k_0^2\hat{s}_2\hat{s}_2' I_2(s_2')G_{22} + \frac{\partial I_2(s_2')}{\partial s_2'}\frac{\partial G_{22}}{\partial s_2}\right]ds_2'\right\}
\end{aligned} \tag{2}$$

where

$$G_{pq} = \frac{e^{-jk_0R_{pq}}}{R_{pq}}$$

and the unit vectors $\hat{s}_1$ and $\hat{s}_2$ are in the direction of the co-ordinates s_1 and s_2, respectively. L_1 and L_2 denote integration over each loop perimeter. The constant $k_0 = 2\pi/\lambda$ is the free-space wavenumber and R_{pq} represents the distance from the observation point on loop p to the source point on loop q, where $p, q = 1, 2$. Although the integrations in eqn. 2 are performed in the local co-ordinates of each antenna, the components of the unit and field vectors must be expressed in the reference co-ordinate system to ensure proper evaluation of the vector inner products. These integral equations can be aug

mented to allow analysis of loops over an infinite ground plane through addition of terms representing the loop image.

When computing the value of R_{pq}, the thin-wire assumption allows the approximation that the observation point is along the wire axis rather than the wire surface. The source point is chosen according to the convention that the point is on the wire surface at $z_p = r_{wp}$ if $p = q$ (r_{wp} = wire radius of loop p), and on the wire axis if $p \neq q$. Use of this convention provides a convenient method for overcoming the difficulties associated with the singular integrand for coincident source and observation points. Computation of the distance R_{pq} is most conveniently performed in the reference co-ordinate system.

3.2 Moment method solution: curved subsections

To apply the integral equations of eqn. 2 to the superquadric geometry, we used the parametric representation developed in Section 8. This involves changing the functions of s to functions of the parameter τ and integrating over the range $0 \leqslant \tau \leqslant 2\pi$. An important feature of the use of this parametric construction for the superquadric loop is that curved wire segments, rather than the commonly used piecewise-linear segments, are implemented to represent the geometry. Recent developments have shown that such a practice proves to be more computationally efficient [15].

The moment method matrix is formed from the integral equations by dividing the curve into discrete segments at the points τ_n, $n = 1$ to N. A Galerkin moment method approach with piecewise sinusoidal subsectional basis and testing functions of the form

$$f_n(\tau) = \begin{cases} \dfrac{\sin(\tau - \tau_{n-1})}{\sin(\tau_n - \tau_{n-1})} & \text{if } \tau_{n-1} \leqslant \tau \leqslant \tau_n \\ \dfrac{\sin(\tau_{n+1} - \tau)}{\sin(\tau_{n+1} - \tau_n)} & \text{if } \tau_n \leqslant \tau \leqslant \tau_{n+1} \\ 0 & \text{otherwise} \end{cases} \quad (3)$$

is then implemented to create the linear system whose unknown vector represents the currents $I_1(s_1)$ and $I_2(s_2)$ on the coupled loop antennas.

The excitation vector in the matrix equation is obtained using either the delta gap or magnetic frill source model. In the delta gap model, the impressed field is assumed constant and to exist only in a small feeding gap in the loop conductor. The field value is given by $\hat{s} \cdot \boldsymbol{E}^{inc} = V/\Delta g$, where Δg is the gap width and V is the impressed feed voltage. In general, Δg is not constrained to equal the subsectional arc length. The magnetic frill source model [6, 21] uses an annular ring of magnetic current at the antenna feed point to represent the excitation from a coaxial line feeding a half loop over a large ground plane. Using image theory, the half loop with the ground plane can be represented as a full loop with the magnetic frill plus its image, as shown in Fig. 3. The inner and outer radii of the annular current ring correspond to the coaxial inner and outer wire radii r_w and a_0, respectively, which are related by $a_0 = 2.3r_w$ for an air-filled 50 Ω coaxial cable. It is important to recognise that the current and input admittance of the half loop are twice those of the full loop antenna model of Fig. 3.

Once the currents $I_1(s_1)$ and $I_2(s_2)$ have been determined from the coupled integral equations, the far-field radiation pattern for the superquadric loops can be obtained from the radiation integral. As shown later, evaluation of the antenna diversity performance of the coupled antennas requires distinction between the contribution from each loop to the overall pattern. Therefore,

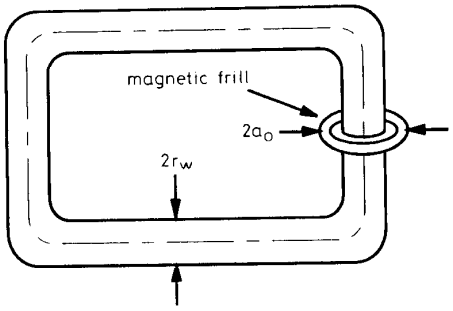

Fig. 3 *Full loop model of half-loop excited by magnetic frill source*

we express the pattern due to each antenna as

$$\boldsymbol{E}_p(\theta, \phi) \simeq \frac{-j\omega\mu_0}{4\pi} \frac{e^{-jkor}}{r} \int_{L_p} I_p(s'_p)\hat{s}'_p \exp(jk_0 \hat{r} \cdot \boldsymbol{r}'_p)\, ds'_p \quad (4)$$

for $p = 1, 2$, where r is the distance from the co-ordinate origin to the field observation distance and $\boldsymbol{r}'_p$ is the position vector as defined in Fig. 2. Once again, the vector components in eqn. 4 should be expressed in the reference co-ordinates to allow proper evaluation of the vector inner products. The total pattern may then be written as the sum

$$\boldsymbol{E}(\theta, \phi) = \boldsymbol{E}_1(\theta, \phi) + \boldsymbol{E}_2(\theta, \phi) \quad (5)$$

4 Mobile communications scenario

One of the objectives of this work is to determine the performance of the coupled superquadric loop antennas when used in a diversity scheme for a mobile communications system. In this application, we are interested in the use of space, angle, and polarisation diversity to combat the effects of short-term or Rayleigh-type fading in a multipath environment. This type of fading occurs when multiple waves with random phases exist simultaneously to produce a spatial interference pattern, causing the received signal strength to vary with antenna position. Antenna diversity operates on the concept that by providing multiple antennas for a single receiver, there is an increased probability that at least one of the antenna elements will receive a signal of adequate strength. Such antenna diversity scenarios are becoming more predominant as communications systems demand increased signal quality and reliability.

Quantitative evaluation of the performance of multiple antennas configured in a diversity arrangement involves investigation of the statistics of the signals received by the elements through examination of the envelope correlation coefficient ρ_e. This quantity provides a measure of the similarity of the voltages at each antenna terminal and should ideally be zero for maximal diversity performance (assuming Rayleigh distributed field strengths). For simplicity, the discussion here is concerned with two antennas only, although additional antennas may be analysed by the same procedure [16–19].

Although the statistical behaviour of the fields in a multipath fading environment as well as the expressions for the correlation coefficient for two antennas have been addressed at length in the literature [16–17], a brief presentation of the key assumptions made in developing these expressions is provided. In all expressions, the variables θ and ϕ are taken with respect to a co-ordinate system

oriented with the z-axis perpendicular to the earth. The following are the basic assumptions applied in the theoretical analysis:

(*a*) The Rayleigh probability density function describes the envelope of the fading signal, leading to zero-mean complex Gaussian descriptions of the voltages received by the two antennas [17].

(*b*) Orthogonal polarisations in the incoming multipath wave are uncorrelated, equally likely, and characterised by power densities per steradian $S_\theta(\theta, \phi)$ and $S_\phi(\theta, \phi)$ for the $\hat{\theta}$ and $\hat{\phi}$ polarisations, respectively.

(*c*) Each individual polarisation is spatially uncorrelated (i.e. wave incoming at (θ, ϕ) is uncorrelated with wave at (θ', ϕ') for $\theta' \neq \theta$ or $\phi' \neq \phi$).

(*d*) The spatial distribution of the incoming multipath waves is limited to the horizontal plane only ($\theta = \pi/2$) and the power density for each wave is a constant over this plane (i.e. $S_\theta(\pi/2, \phi) = S_\theta^0 = \text{constant}$ and $S_\phi(\pi/2, \phi) = S_\phi^0 = \text{constant}$).

Using these assumptions leads to an expression for the envelope correlation coefficient for the signals received by the two antennas which assumes the form [16]

$$\rho_e = \frac{\left| \int_0^{2\pi} \boldsymbol{E}_1(\pi/2, \phi) \cdot \boldsymbol{E}_2^*(\pi/2, \phi)\, d\phi \right|^2}{\int_0^{2\pi} |\boldsymbol{E}_1(\pi/2, \phi)|^2\, d\phi \int_0^{2\pi} |\boldsymbol{E}_2(\pi/2, \phi)|^2\, d\phi} \tag{6}$$

where $\boldsymbol{E}_p(\theta, \phi) = E_{\theta p}(\theta, \phi)\hat{\theta} + E_{\phi p}(\theta, \phi)\hat{\phi}$ is the vector radiation pattern associated with antenna p obtained from eqn. 4 for the case of the coupled loop antennas.

There arises some question concerning precisely which currents to use to obtain the patterns $\boldsymbol{E}_p$ in eqn. 6. For instance, isolated or coupled loop configurations may be used in the computation for the current on each loop. If a coupled loop configuration is used, the second antenna may be either excited or terminated in an open circuit or matched load. In the examples shown in this work, the currents on each antenna are computed by using identical excitations for both antennas. This scheme fully includes the effects of mutual coupling on the antenna current behaviour. The currents obtained are subsequently placed in eqn. 4 to compute the patterns associated with each loop.

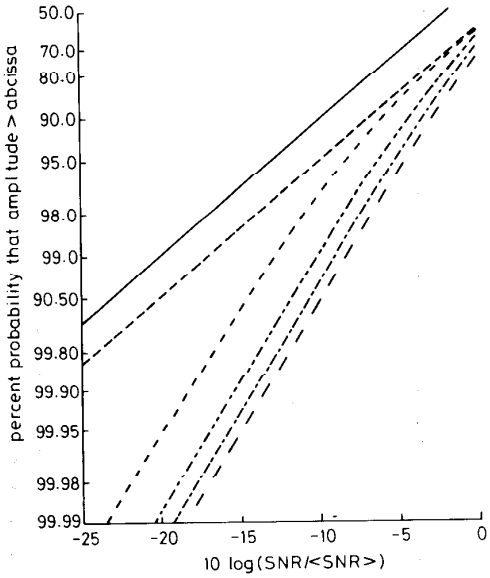

Fig. 4 *Probability distribution of received SNR for two-branch maximal ratio combining for different values of envelope correlation coefficient ρ_e*

——— Rayleigh ------- $\rho_e = 0.9$ —·—·— $\rho_e = 0.3$
– – – – $\rho_e = 1.0$ —··—·· $\rho_e = 0.6$ — — — $\rho_e = 0.0$

Fig. 4 shows the cumulative probability distribution of the signal-to-noise ratio (SNR) normalised to its average ($\langle$SNR$\rangle$) for various values of ρ_e and for two-antenna diversity. Maximal ratio combining in which the two signals are received, cophased, properly weighted, and added is assumed in this plot. Also shown is the Rayleigh distribution which corresponds to a single antenna in the multipath environment. As can be seen, reduction of the envelope correlation coefficient provides a considerable increase in the probability of receiving a signal of adequate strength for reliable communication. In light of this, the goal in diversity antenna design is to minimise this factor to the extent possible using a combination of spatial, angle, and polarisation diversity.

5 Computational examples

The preceding developments can be used to perform some computational studies on the characteristics of coupled superquadric loop antennas. Throughout this Section a wire radius r_w is used such that

$$\Omega_0 = 2 \ln \frac{P}{r_w} = 10 \tag{7}$$

is satisfied, where P is the loop perimeter. Five-point Gaussian quadrature integration is used to evaluate the integrals over each subsection. Where the magnetic frill generator source is implemented, the frill dimensions are chosen to match those of a 50 Ω feeding coaxial line. Numerical tests of the moment method algorithm were performed to ensure that small enough subsections were used to obtain convergent values for the input impedance.

5.1 Parallel circular loops

Before demonstrating the versatility of the computational model, it is interesting to investigate the correspondence between the results of this work and previously obtained results for parallel circular coupled loop antennas. Fig. 5 illustrates a typical plot of self and mutual admittance against separation z_0 for the case of two circular loops with circumferences P of 0.2λ, 0.4λ, 0.6λ, and 0.8λ. The magnetic frill source was used for the configuration shown in the inset of Fig. 5*a*. This plot indicates the increase in mutual coupling with increased loop dimensions characterised by higher mutual admittance values and more pronounced admittance variation with separation distance. Also noteworthy is the reduction in mutual admittance with increased separation, resulting in self admittances which asymptotically approach the input admittance values for isolated loops of $0.00603 - j3.36$, $0.0370 - j0.494$, $0.173 + j1.28$, and $0.900 + j3.38$ mS for loop sizes of 0.2λ, 0.4λ, 0.6λ, and 0.8λ, respectively. Finally, this computation illustrates the low admittance (high impedance) values which result in the impedance matching problem for loops near 0.5λ. The dots in the Figure are values taken from a study by Iizuka *et al.* [8]. It is clear that excellent agreement is obtained between the two sets of results over a wide range of loop sizes and separations. This comparison supports the model's capability to faithfully reproduce the results of previous studies and provides insight into the effect of antenna separation on the mutual admittance of the coupled loops.

5.2 Current distribution

When two superquadric loop antennas are operating in close proximity to each other, it is expected that the

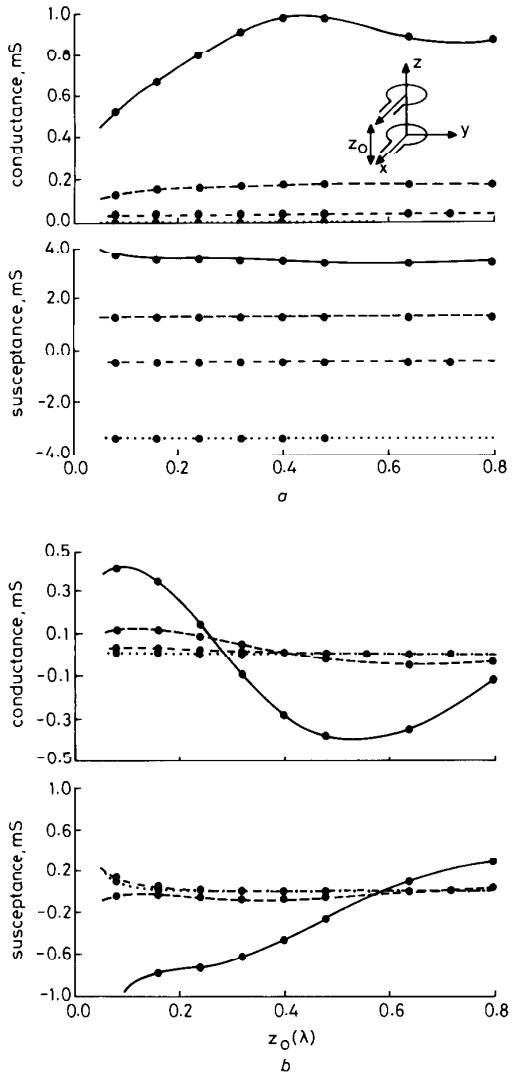

Fig. 5 *Self admittance against separation distance for parallel circular loops with different loop circumferences P*

a Self admittance
b Mutual admittance
——— $P = 0.8\lambda$
– – – – $P = 0.6\lambda$
------- $P = 0.4\lambda$
····· $P = 0.2\lambda$
●●● Reference 8

mutual coupling will affect the current distribution along the wires. Fig. 6 illustrates this effect for a nearly rectangular 0.8λ loop with $v = 30$ and $b/a = 2$. The current magnitude is normalised to the antenna input voltage. In this example, the solid line represents the current magnitude and phase for the loop when it operates in phase with an identical loop located $z_0 = 0.2\lambda$ from and parallel to the antenna. The dashed line represents the current distribution for the same loop operating in an isolated environment. As can be seen, although the general behaviour of the current is unchanged, the levels and detailed variation of the current are noticeably influenced by the presence of the second antenna. Especially noteworthy is the substantial decrease in the current magnitude along the wire near the point opposite the feed at $s = 0.4\lambda$.

5.3 Loops near an infinite ground plane

One of the practical uses of the loop is in communications equipment, where the loop may possibly be near a

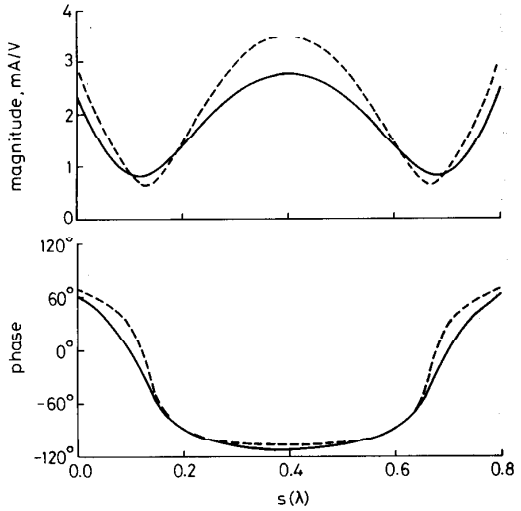

Fig. 6 *Current distribution against perimeter co-ordinate s for a 0.8λ loop ($v = 30$, $b/a = 2$) parallel to and located $z_0 = 0.2\lambda$ from identically shaped and excited antenna compared to that of isolated loop*

——— coupled loops
– – – – isolated loop

finite-size conducting plate or other body. A first-order approximation of the behaviour of the loop in this environment may be obtained by solving the problem for the loop near an infinite ground plane. For example, Fig. 7*a* shows a 0.2λ nearly rectangular ($v = 50$) loop located $c = 0.01\lambda$ from an infinite planar conductor for three different positions of the source. The variation of the input impedance versus the aspect ratio b/a is illustrated in Fig. 7*b* for a delta gap generator with $\Delta g = 0.003\lambda$. It is evident that both the source location and the aspect ratio play a role in determining the loop input impedance for this configuration.

Fig. 8 shows the far-field radiation patterns obtained for a 0.25λ elliptical loop ($v = 2$) of aspect ratio $b/a = 2$ oriented parallel to and located 0.1λ from the ground plane as illustrated in the inset. For comparison, the pattern for the same loop isolated from the ground plane is also provided. The patterns are normalised to represent the antenna directivity and are shown for the principal planes only. As is expected, the presence of the conducting sheet results in a null field at $\theta = 90°$ and noticeably increases the boresight antenna directivity. The E_θ component in the $\phi = 0°$ cut is not included because it experiences a null in this plane. Table 1 compares the input impedance and total real power radiated by the loop in Fig. 8 for the isolated and ground plane configurations. As expected, the presence of the ground plane significantly reduces the total power radiated by the loop antenna.

Table 1: Input impedance and radiated power (normalised to square of input voltage) comparison for loop configurations of Fig. 8

Configuration	Input impedance	Radiated power
		mW/V²
Ground plane	$0.267 + j383.94\ \Omega$	0.0543
Isolated	$1.382 + j385.65\ \Omega$	0.279

5.4 Concentric loops

In many systems, multiple loop antennas may be positioned such that they are in a concentric configuration.

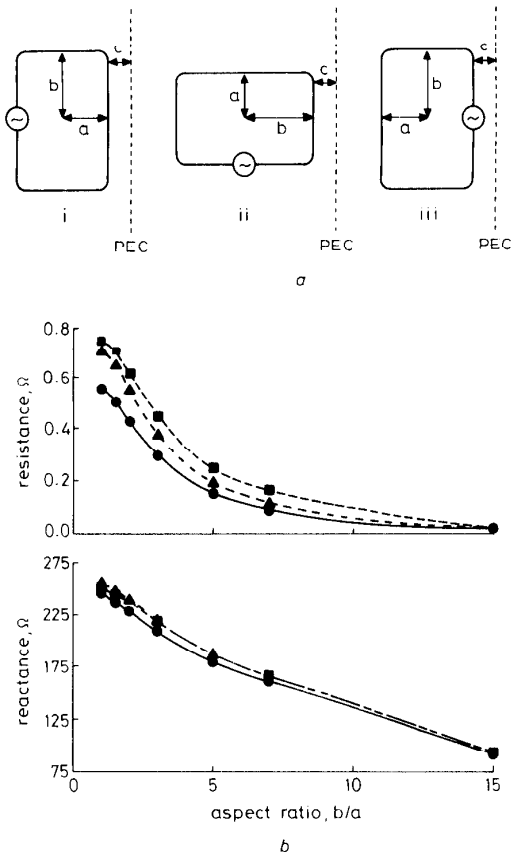

Fig. 7 *0.2λ loop with v = 50 located c = 0.01λ from infinite conducting plane for three source positions*

a Geometry
b Input impedance against aspect ratio *b/a* for three cases shown
●—● case i
■—■ case ii
▲—▲ case iii

An example of this type of situation is illustrated in the inset of Fig. 9, where the larger and smaller loops each have a 0.25λ perimeter at their operating frequencies of f_0 and $3f_0$, respectively. The loops have aspect ratios of $b/a = 1$ and are excited using a delta-gap source model. For these computations, each loop is in turn excited at its operating frequency while a short circuit is placed across the terminals of the other loop. The curves in Fig. 9 compare the variation in the input impedance versus the squareness parameter v for each loop as well as that of an isolated 0.25λ loop. From these results, we conclude that the presence of the second loop has a significant effect on the impedance values. This plot further illustrates the role of the loop squareness in determining its terminal impedance. These results can be very useful in the design of coupled loop antennas for communications applications.

A second interesting configuration is shown in the inset of Fig. 10 where two loops are arranged in a cross geometry and placed at $z_0 = 0.26\lambda$ above an infinite ground plane. Each loop is fed using a delta gap source model and has superquadric parameters of $v = 10$ and $a = 2.5b = 0.125\lambda$. Fig. 10*a* and *b* provide the far-zone radiation patterns in dB normalised to represent the antenna directivity in the xz (or yz) and xy-planes, respectively, when the two loops are fed in phase. Fig. 10*c* and *d* provide the directivity patterns in dB in the xy-plane for the same configuration when the two loops are

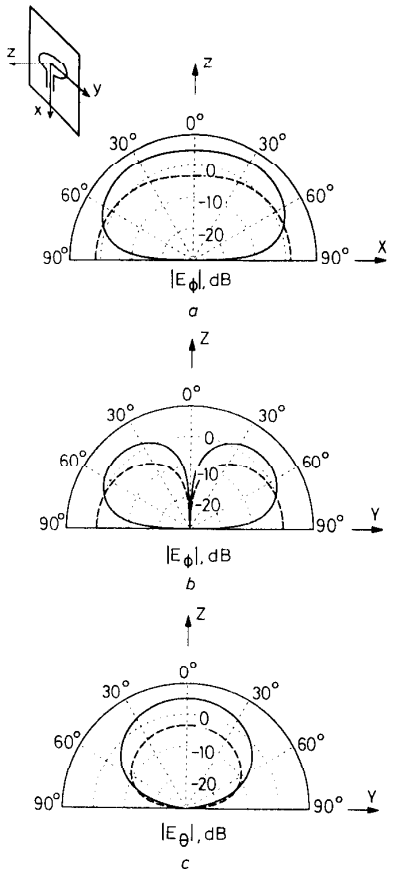

Fig. 8 *Directivity pattern for 0.25λ elliptical loop of aspect ratio b/a = 2 both isolated and located 0.1λ from infinite ground plane*

a ϕ-polarisation, $\phi = 0°$ plane (E_θ is null)
b ϕ-polarisation, $\phi = 90°$ plane
c θ-polarisation, $\phi = 90°$ plane
——— ground plane
- - - - isolated

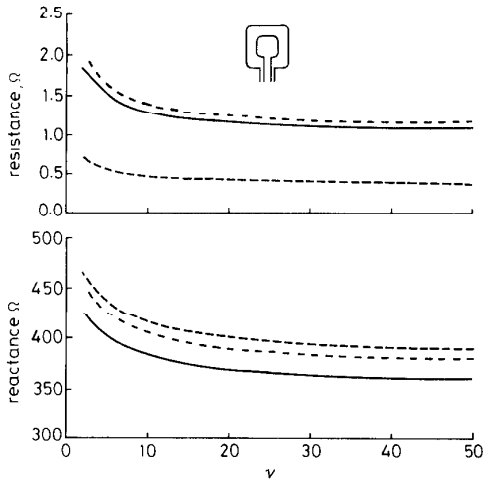

Fig. 9 *Input impedance against squareness parameter v for concentric 0.25λ loops with b/a = 1 compared with that of isolated loop*

Larger and smaller loops operate at f_0 and $3f_0$, respectively
——— single loop
- - - - small loop
------- large loop

fed 45° and 90° out of phase, respectively. As can be seen, through proper variation of the feeding voltages, the antenna radiation pattern can be made to be omnidirectional in the horizontal plane.

Fig. 12 illustrates the effects of antenna rotation on the envelope correlation coefficient for the 0.25λ loop with $v = 10$ and $b/a = 1$. Results for antenna separations y_0 of 0.1λ, 0.2λ, 0.3λ, and 0.4λ are given as a function of the

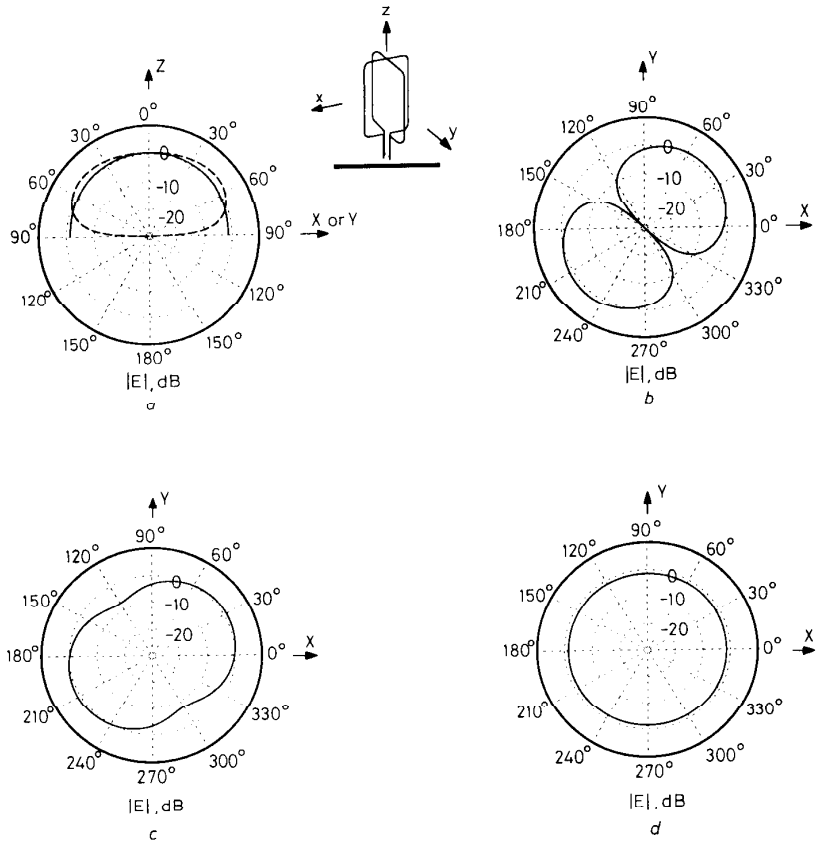

Fig. 10 *Directivity patterns in dB for two crossed superquadric loops at $z_0 = 0.26\lambda$ over infinite ground plane with $v = 10$ and $a = 2.5b = 0.125\lambda$*

a *xz*-plane pattern with loops excited in phase
b *xy*-plane pattern with loops excited in phase
c *xy*-plane pattern with loops excited 45° degrees out of phase
d *xy*-plane pattern with loops excited 90° degrees out of phase
——— E_θ
- - - - E_ϕ

5.5 Diversity

The diversity performance of small antennas is an important consideration in the design of personal communications networks. To determine the diversity performance of a given antenna configuration, the loops are each excited with the same feed voltage and the currents are determined using the formulation presented in this paper. The envelope correlation coefficient is then computed using eqn. 6 in conjunction with eqn. 4. Fig. 11 provides a plot of the envelope correlation coefficient as a function of loop separation y_0 for the case of two parallel loops as depicted in the inset. In this Figure, the solid line represents ρ_e for two antennas with isotropic patterns in the xy-plane [19]. The remaining curves show ρ_e for loops with perimeters 0.25λ, 0.50λ, 0.75λ, and 1.0λ with $v = 10$ and $b/a = 1$. This plot demonstrates the well known theortical zero in the correlation coefficient for antenna spacings near 0.4λ, which would therefore be the ideal operating point. However, in smaller systems where this separation is not physically possible, reasonable diversity performance can still be achieved for spacings as low as 0.15λ where $\rho_e \sim 0.7$

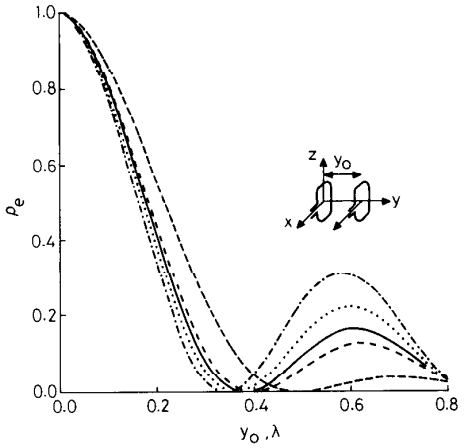

Fig. 11 *Envelope correlation coefficient against separation distance for loops of perimeter P with $b/a = 1$ and $v = 10$ compared with that of two antennas with isotropic patterns in horizontal plane*

——— isotropic
- - - - $P = 0.25\lambda$
------- $P = 0.50\lambda$
····· $P = 0.75\lambda$
—·—· $P = 1.00\lambda$

rotation β of the second loop while the first loop is held stationary. As the antenna rotates, angle and polarisation

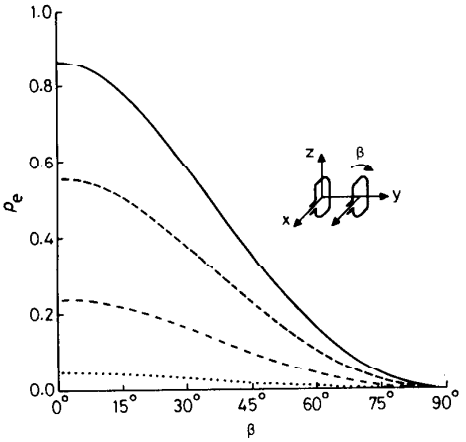

Fig. 12 *Envelope correlation coefficient against rotation angle for 0.25λ loops with b/a = 1 and v = 10 for various separation distances*

—— $y_0 = 0.1\lambda$
– – – – $y_0 = 0.2\lambda$
------ $y_0 = 0.3\lambda$
····· $y_0 = 0.4\lambda$

diversity result in a dramatic decrease in the signal correlation. Such an arrangement of antennas can be a useful means of achieving high diversity returns in mobile units where space is an important consideration, and in fact has been implemented in some cases [17, p. 148].

6 Conclusion

In this work we have presented the development of a computational model of two coupled loop radiators with arbitrary relative orientation and position. Use of the superquadric curve to represent the loop geometries allows investigation of a large range of practical antennas, including circular, elliptical, and rectangular loops, using one general analysis. A Galerkin method of moments technique with piecewise sinusoidal subsectional basis functions has been applied to solve the electric field integral equation for thin wires using a parametric representation of the superquadric loop. This construction allows the antenna to be represented with curved rather than piecewise linear subsectional segments, resulting in a computationally efficient algorithm. The current distribution in the loops computed from the integral equation is subsequently used to obtain the antenna self, mutual, and input impedance and directivity pattern. Several representative results have been given which not only provide insight into the effects of such factors as the loop squareness and aspect ratio on the antenna behaviour but also show the model's versatility in analysing many different types of structures. These examples further allow determination of the effect of placing the two loops in close proximity to each other as might occur in mobile communications applications. In many cases where the system configuration places constraints on the antenna shape, size, and position, incorporation of this formulation in the design process can help in determining the most suitable configuration to meet the needs of the system.

We have also discussed the concept of antenna diversity and have presented the expression for computing the envelope correlation coefficient for signals received by multiple antennas. This expression was applied to several coupled loop arrangements to illustrate the potential diversity performance of these radiators when used in a proper configuration. We have shown that with proper orientation and spacing, good diversity action can be obtained even for antennas which are spaced closely together. This information is crucial to the development of robust mobile receiver units designed for use in a multipath environment.

7 References

1 POCKLINGTON, H.C.: 'Electrical oscillations in wires', *Proc. Cambridge Phil. Soc.*, 1897, **9**, pp. 324–332
2 HALLÉN, E.: 'Theoretical investigations into transmitting and receiving qualities of antennae', *Nova Acta Regiae Soc. Sci. Ups., Ser. 4*, 1938, **11**, pp. 1–44
3 STORER, J.E.: 'Impedance of thin-wire loop antennas', *Trans. Am. Inst. Electr. Eng.*, 1956, **75**, pt. 1, pp. 606–619
4 WU, T.T.: 'Theory of the thin circular loop antenna', *J. Math. Phys.*, 1962, **3**, pp. 1301–1304
5 HARRINGTON, R.F., and MAUTZ, J.: 'Electromagnetic behaviour of circular wire loops with arbitrary excitation and loading', *Proc. IEE*, Jan. 1968, **115**, (1), pp. 68–77
6 ZHOU, G., and SMITH, G.S.: 'An accurate theoretical model for the thin-wire circular half-loop antenna', *IEEE Trans.*, 1991, **AP-39**, (8), pp. 1167–1177
7 ADACHI, S., and MUSHIAKE, Y.: 'Theoretical formulation for circular loop antennas by integral equation method', *Sci. Rep. Res. Inst. Tohoku Univ. Ser. B*, 1957, **9**, pp. 9–18
8 IIZUKA, K., KING, R.W.P., and HARRISON, C.W.: 'Self- and mutual admittances of two identical circular loop antennas in a conducting medium and in air', *IEEE Trans.*, 1966, **AP-14**, (4), pp. 440–450
9 ABUL-KASSEM, A.S., and CHANG, D.C.: 'On two parallel loop antennas', *IEEE Trans.*, 1980, **AP-28**, (4), pp. 491–496
10 TSUKIJI, T., and TOU, S.: 'On polygonal loop antennas', *IEEE Trans.*, 1980, **AP-28**, (4), pp. 571–575
11 BAKER, K., and LAGRONE, A.H.: 'Digital computation of the mutual impedance between thin dipoles', *IRE Trans.*, 1962, **AP-10**, pp. 172–178
12 BARR, A.H.: 'Superquadrics and angle-preserving transformations', *IEEE Comput. Graph. Appl.*, 1981, **1**, pp. 11–23
13 HARRINGTON, R.F.: 'Field computation by moment methods' (Macmillan, New York, 1968)
14 POGGIO, A.J., and MILLER, E.K.: 'Techniques for low-frequency problems', *in* LO, Y.T., and LEE, S.W. (Eds.): 'Antenna handbook: theory, applications, and design' (Van Nostrand Reinhold, New York, 1988), Chap. 3
15 CHAMPAGNE, N.J., WILLIAMS, J.T., and WILTON, D.R.: 'The use of curved segments for numerically modeling thin-wire antennas and scatterers', *IEEE Trans.*, 1992, **AP-40**, (6), pp. 682–689
16 VAUGHAN, R.G., and ANDERSEN, J.B.: 'Antenna diversity in mobile communications'. *IEEE Trans. Veh. Technol.*, 1987, **VT-36**, (4), pp. 149–172
17 JAKES, W.C.: 'Microwave mobile communications' (Wiley, New York, 1974)
18 LEE, W.C.Y.: 'Mobile communications engineering' (Wiley, New York, 1982)
19 CLARKE, R.H.: 'A statistical theory of mobile radio reception', *Bell Syst. Tech J.*, 1969, **47**, pp. 957–1000
20 RAHMAT-SAMII, Y.: 'Useful coordinate transformations for antenna applications', *IEEE Trans.*, 1979, **AP-27**, pp. 571–574
21 TSAI, L.L.: 'A numerical solution for the near and far fields of an annular ring of magnetic current', *IEEE Trans.*, 1972, **AP-20**, (5), pp. 569–576

8 Appendix

8.1 Superquadric parametrisation

To permit the use of curved subsectional wire segments in the moment method analysis of superquadric loop antennas, it is necessary to first parametrise the curve in a convenient form. Among the many parametrisations possible, observation has shown that a form which provides mathematical simplicity and numerical stability uses the parameter τ and assumes the form

$$x = a\psi(\tau)\cos\tau \tag{8}$$

$$y = b\psi(\tau)\sin\tau \tag{9}$$

where

$$\psi(\tau) = \frac{1}{(|\sin\tau|^{\nu} + |\cos\tau|^{\nu})^{1/\nu}} \tag{10}$$

and $0 \leq \tau \leq 2\pi$. The unit tangent vector $\hat{s}$ in the direction of the perimeter co-ordinate s is

$$\hat{s} = \frac{-a|\sin\tau|^{\nu-1}\,\mathrm{sgn}(\sin\tau)}{\gamma(\tau)}\hat{x} + \frac{b|\cos\tau|^{\nu-1}\,\mathrm{sgn}(\cos\tau)}{\gamma(\tau)}\hat{y} \tag{11}$$

where

$$\gamma(\tau) = \sqrt{(a^2|\sin\tau|^{2\nu-2} + b^2|\cos\tau|^{2\nu-2})} \tag{12}$$

The differential arc length ds in terms of the differential $d\tau$ is expressed by

$$ds = |\boldsymbol{r}_{\tau}|\,d\tau = \gamma(\tau)\psi^{\nu+1}(\tau)\,d\tau = \Delta(\tau)\,d\tau \tag{13}$$